JACS
JOURNAL OF THE AMERICAN CHEMICAL SOCIETY
pubs.acs.org/JACS
Article

Cavity Manipulation of Attosecond Charge Migration in Conjugated Dendrimers

Baicheng Zhang, Yonghao Gu,* Victor Manuel Freixas, Shichao Sun, Sergei Tretiak, Jun Jiang,* and Shaul Mukamel*

Cite This: J. Am. Chem. Soc. 2024, 146, 26743−26750
Read Online
ACCESS | Metrics & More | Article Recommendations | Supporting Information

ABSTRACT: Dendrimers are branched polymers with wide applications to photosensitization, photocatalysis, photodynamic therapy, photovoltaic conversion, and light sensor amplification. The primary step of numerous photophysical and photochemical processes in many molecules involves ultrafast coherent electronic dynamics and charge oscillations triggered by photoexcitation. This electronic wavepacket motion at short times where the nuclei are frozen is known as attosecond charge migration. We show how charge migration in a dendrimer can be manipulated by placing it in an optical cavity and monitored by time-resolved X-ray diffraction. Our simulations demonstrate that the dendrimer charge migration modes and the character of photoexcited wave function can be significantly influenced by the strong light-matter interaction in the cavity. This presents a new avenue for modulating initial ultrafast charge dynamics and subsequently controlling coherent energy transfer in dendritic nanostructures.

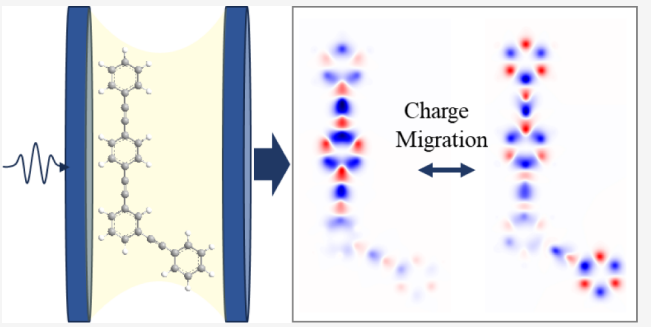

INTRODUCTION

Dendrimers are branched tree-like polymers,[1] which have drawn significant interest as photosensitizers[2] and photocatalysts,[3] due to their distinct structure and versatile functionality.[1] The crux of a dendrimer's utility lies in its unique branched tree-like architecture, which shows a high degree of surface functionality coupled with internal pockets and enables them to engage with a diverse array of molecular entities effectively. In photodynamic therapy, for instance, dendrimers serve as vehicles to transport photosensitizers to specific body regions, offering a targeted approach to cancer treatment.[4] Similarly, in photovoltaics, conjugated denstimers potentially enhance solar cell efficiency by facilitating improved light absorption and directed carrier transport utilizing antenna-like cascading principles.[5−8]

Extensive efforts have been dedicated to improving optoelectronic and light harvesting functions of dendrimers through the optimization of their topologies, structural rigidity, and electronic-vibrational (vibronic) couplings.[9−11] For instance, initial investigations revealed the pivotal role of building block connectivity and topology in dendritic structures.[12] Here connectivity through a meta-position of a central benzene ring often constrains electronic communications leading to appearance of Frenkel-like excitonic states[13] followed by a picosecond Förster resonance energy transfer (FRET). In contrast, para- and ortho- type linkages facilitate the formation of more delocalized electronic states approaching the Wannier exciton limit,[13] potentially resulting in more efficient energy transfer with coherent characteristics.[14,15] It is established that photoexcited dynamics in dendrimers can be well controlled using pulse-shaping techniques.[10] It is intriguing to explore the early stages of electronic dynamics that shape the initial photoexcited wavepacket in dendrimers.

Modern attosecond science makes it possible to probe charge migration, which involves ultrafast charge oscillations caused by the electronic coherence when a molecule is photoexcited or photoionized into a superposition of electronic states. These dynamics occur on time scales of a few femtoseconds when nuclei remain essentially frozen.[16−20] Charge migration is the early stage of many charge and energy transfer processes and charge-induced reactions, playing an important role in the efficiency of these photophysical and photochemical processes.[21−23] Investigating charge migration in dendrimers is of particular interest, given the complex interplay between their branched structure and electronic states.[10−12]

Optical cavities provide potent means to manipulate charge migration in dendrimers. Molecules coupled to an optical cavity can interact with the vacuum field of the cavity photon

Received: May 16, 2024
Revised: August 29, 2024
Accepted: August 30, 2024
Published: September 18, 2024

mode even without external driving fields, forming hybrid light-matter states known as polaritons.[24−31] Optical cavities can be characterized by the effective radiation matter coupling strength $\kappa = \mu\sqrt{\hbar\omega_c/2\varepsilon_0 V_c}$, where μ is the transition dipole moment, ε_0 is the vacuum electric permittivity, V_c is the cavity mode volume and ω_c is the cavity frequency. The cavity mode can be characterized by the ratio of the cavity frequency to the resonance width, known as the quality factor (Q). A larger Q indicates higher quality and a longer cavity photon lifetime. Theoretical and experimental studies have shown that photophysical and photochemical processes such as chemical reactivity, reaction rates and long-range energy transfer can be altered by creating polaritons.[32−43]

Here, we investigate the effects of optical cavities on charge migration in conjugated dendrimer molecules that are photoexcited into a superposition of electronic states. Our target systems include meta-connectivity between dendritic branches that weakens the π electronic conjugation. In this case electronic states are spatially localized,[13] which brings barriers to electron and hole migration between branches of the bare dendrimer. We find that interbranch exciton passage becomes possible by placing the dendrimer in an optical cavity that facilitates mixing of the electronic states and enables transitions between them. We further simulate the heterodyne-detected time-resolved X-ray diffraction (TR-XRD) signal for monitoring this process.[44,45] Polariton effects are clearly observed. These findings suggest a novel approach to control the initial charge dynamics in conjugated dendrimers, offering potential applications across photochemistry and photophysics. This could potentially enhance the light harvesting efficacy, elevate the performance of optoelectronic devices, and bolster sensor capabilities.

PROBING ELECTRONIC DYNAMICS BY TIME-RESOLVED X-RAY DIFFRACTION

Our molecules are described by the Hamiltonian $H_{\mathrm{Mol}}=\sum_i \hbar\omega_i |i\rangle\langle i|$, where index i labels ground ($i = 0$) and relevant excited ($i > 0$) states. The molecule is then photoexcited into a superposition of electronic states. The excited state dynamics are computed through numerical solutions of the time dependent Schrödinger equation. The time-dependent electronic charge density is given by

$$\sigma^E_{\mathrm{total}}(\boldsymbol{r}, t) = \sum_i \rho_{ii}\sigma^E_{ii}(\boldsymbol{r}) + \sum_{i\neq j} \rho_{ij}(t)\sigma^E_{ij}(\boldsymbol{r}) \tag{1}$$

where $\boldsymbol{r}$ is the spatial coordinate and $\sigma^E_{ii}(\boldsymbol{r})$ and $\sigma^E_{ij}(\boldsymbol{r})$ are the state and the transition charge density between electronic states i and j, respectively. In this study, the nuclei are assumed frozen over the attosecond charge migration time scale. The electronic populations ρ_{ii} become time-independent after the pump excitation, while the electronic coherences $\rho_{ij}(t)$ oscillate at frequency corresponding to the energy difference of states i and j.

The total Hamiltonian of the molecule coupled to a single cavity mode is given by

$$H = H_{\mathrm{Mol}} + H_{\mathrm{Cav}} + H_{\mathrm{MolCav}} \tag{2}$$

where the cavity Hamiltonian is $H_{\mathrm{Cav}} = \hbar\omega_c\left(a^\dagger a + \frac{1}{2}\right)$ and a and $a^\dagger$ are the cavity mode annihilation and creation operators, respectively. The interaction between the molecule and the cavity is characterized within the electronic dipole approximation $H_{\mathrm{MolCav}}=-\boldsymbol{\mu}\cdot\boldsymbol{E}_c(\boldsymbol{r})$, where

$$\boldsymbol{E}_c(\boldsymbol{r}) = i\sqrt{\hbar\omega_c/2\varepsilon_0 V_c}\, a e^{i\boldsymbol{k}_c\cdot\boldsymbol{r}}\boldsymbol{e}_c + H.\,c. \tag{3}$$

where $\boldsymbol{k}_c$ is the cavity-mode wave vector, $\boldsymbol{e}_c$ is the field polarization, and $H.c.$ stands for the Hermitian conjugate. The cavity coupling strength is $g = \sqrt{\hbar\omega_c/2\varepsilon_0 V_c}$. The polariton states $\{|P_k\rangle\}$ are calculated by diagonalizing the polaritonic Hamiltonian using the direct product basis set $|i,n\rangle=|i\rangle\otimes|n\rangle_c$, where $\{|n\rangle_c\}$ is the Fock states of the cavities photons.

The attosecond charge migration is monitored by a TR-XRD movie. The heterodyne-detected attosecond X-ray diffraction signal is given by

$$S_{\mathrm{het}}(\boldsymbol{q}) \propto 2\Im\int \mathrm{d}t \boldsymbol{A}_{\mathrm{het}}(t)\boldsymbol{A}_X(t)\sigma(\boldsymbol{q}, t) \tag{4}$$

where $\boldsymbol{A}_{het}(t)$ and $\boldsymbol{A}_X(t)$ are envelopes of two coincident X-ray pulses with a controlled relative phase. The diffraction signal time resolution is therefore determined by the duration of the attosecond X-ray probe pulses. $\sigma(\boldsymbol{q},t)$ is the spatial Fourier transform of the charge density:

$$\sigma(\boldsymbol{q}, t) = \int \mathrm{d}\boldsymbol{r} e^{-i\boldsymbol{q}\cdot\boldsymbol{r}}\sigma(\boldsymbol{r}, t) \tag{5}$$

where $\boldsymbol{q}$ is the scattering vector. The charge migration process can be visualized as the time-dependent difference charge density, which is the difference between the time-dependent charge density of the excited molecule and the ground state $\sigma^E_{\mathrm{diff}}(\boldsymbol{r}, t) = \sigma_{\mathrm{total}}(\boldsymbol{r}, t) - \sigma^g_{\mathrm{total}}(\boldsymbol{r})$. Thanks to the linear dependence of the heterodyne XRD signal on the charge densities, the corresponding difference signal can be obtained by $S_{\mathrm{het}}(\sigma^E_{\mathrm{diff}}) = S_{\mathrm{het}}(\sigma_{\mathrm{total}}) - S_{\mathrm{het}}(\sigma^g_{\mathrm{total}})$.

RESULTS AND DISCUSSION

We first consider the conjugated dendrimer $C_{30}H_{18}$ shown in Figure 1a. We adapt the electronic structure description provided by the NEXMD package as detailed in Method section. Charge migration is commonly triggered by ionizing the systems into cations. In this study, instead of photoionization, we photoexcite the molecule into a superposition of electronic states and investigate the following electron and hole dynamics. A linearly polarized Gaussian pulse $\boldsymbol{E}(t) = A\vec{\boldsymbol{e_0}}e^{-i\omega_0 t}e^{-(t^2/2\sigma^2)}$ with a peak amplitude $A = 3.60 \times 10^7$ V/cm, $\sigma = 1.0$ fs duration, central frequency $\omega_0 = 3.30$ eV is used for initialization. These parameters were selected to ensure effective population of the relevant excited states (with largest absorption cross sections) while minimizing the ionization and other nonlinear effects that could complicate the desired charge migration dynamics. Specifically, the central frequency ω_0 was tuned to the average energy of the first and second excited states of the system ($e_1 = 3.23$ eV, $e_2 = 3.56$ eV), ensuring efficient coupling to these states. The pulse duration and amplitude were optimized to provide a balance between efficient excitation and minimal perturbation of the system while demonstrating maximal contrast between there and polaritonic states (see Figure S2). We include the nine relevant excited states and numerically solve the time dependent Schrödinger equation using the fourth-order Runge−Kutta method with 0.03 fs time step. The simulated 6 fs electronic population dynamics triggered by the 1.0 fs pump excitation is shown in Figure 1b. Owing their strong

https://doi.org/10.1021/jacs.4c06727
J. Am. Chem. Soc. 2024, 146, 26743−26750

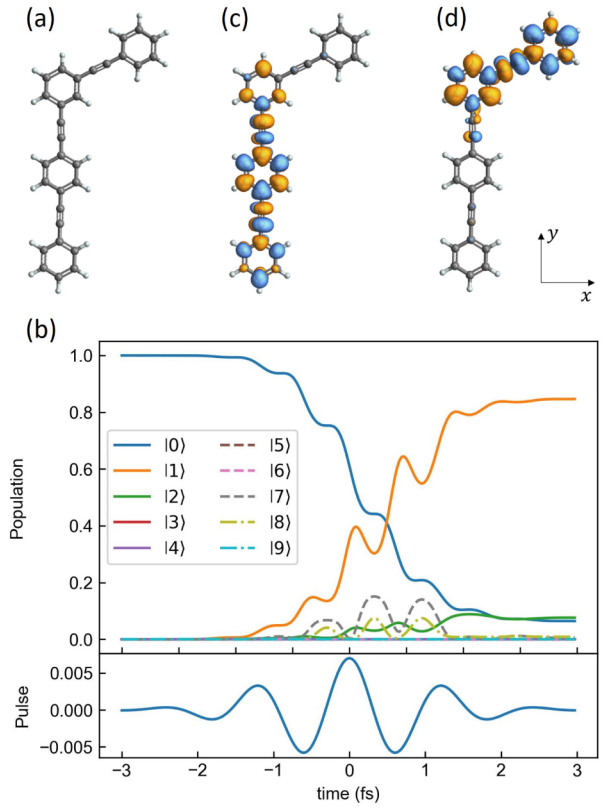

Figure 1. (a) Structure of the dendrimer $C_{30}H_{18}$. (b) Population dynamics of $C_{30}H_{18}$ excited by pump pulse of energy ω_0 = 3.30 eV and duration σ = 1.0*fs*. (c) Transition density from ground state $|0\rangle$ to excited state $|1\rangle$. (d) Transition density from ground state $|0\rangle$ to excited state $|2\rangle$.

transition dipole moments, two excited states are significantly populated. $|1\rangle$ becomes dominant with a population of 0.8, whereas state $|2\rangle$ population reaches 0.1. To display the charge differences of these two states with respect to the ground state, the transition charge densities $\sigma_{ij}^{E}(\boldsymbol{r})$ between the ground state $|0\rangle$ and $|1\rangle$ and $|2\rangle$ are calculated through $\langle 0|\hat{\sigma}|i\rangle$, where $\hat{\sigma}$ is the density operator. As shown in Figure 1c, $\sigma_{01}^{E}(\boldsymbol{r})$ spans the long dendrimer branch. In contrast, $\sigma_{02}^{E}(\boldsymbol{r})$ is localized at the short branch as illustrated in Figure 1d. Different charge migration modes involving states $|1\rangle$ and $|2\rangle$ lead to distinct charge dynamics along different branches.

We have first simulated the charge dynamics of the bare dendrimer molecule and visualized it by the time-dependent difference charge density. Figure 2a-f shows the difference charge densities at selected times *t*. The charge only migrates along the long branch and there is no significant migration to the short branch. This is consistent with previous studies, that showed that meta-substitution can block interbranch electronic communications.[13] Figure 2m-r shows the difference charge densities of the molecule in an optical cavity with coupling strength g = 0.103 V/Å and ω_c = 3.559 eV at selected times *t*. In contrast to the bare molecule, the charge dynamics of the short branch is now significant. Charge migration enabled by polaritonic effects exhibits long-range character spanning the entire molecule. We systematically varied the coupling strength to explore its modification of the charge migration pathways, which change gradually with the coupling strength. As shown in Figure 2g-l, with g = 0.0514 *V*/Å, the charge migration process does not significantly vary by the cavity (Figure 2a-f). As the coupling strength is increased, remarkable changes in the charge migration pathway emerge with the short branch of the dendrimer activated.(Figure 2m-x). Note that the coupling strengths employed here are about 1%−3% of the cavity frequency, which are experimentally feasible. Recent publications have reported the realization of single-molecule strong coupling using plasmonic nanocavities with coupling strengths that are commensurate with those we used in our simulations.[46] Plasmonic cavities often exhibit high losses and broad line widths. Their *Q* factors typically range between 5 and 20.[47] To further explore the loss rate influence of optical cavities on the attosecond charge migration, charge dynamics of cavity modified dendrimers with different *Q* factors were simulated and presented in Figure S9. We emphasize that the charge migration process is not disturbed even with a *Q* factor lower to 10 due to the ultrafast time scale of pure electronic dynamics. Another factor that may influence the charge migration is the coupling of high photon cavity modes. Simulations of the charge dynamics of photoexcited dendrimer with the two-photon mode included in our Hamiltonian are presented in Figure S10. The charge dynamics is identical to those of the single-photon mode calculations. We demonstrate that these effects can be neglected in our simulations because of the off resonance of the high photon modes with the dendrimer electronic states.

To further interpret these findings, we have calculated the population dynamics of the electronic states for different coupling strengths. As shown in Figure 3a, upon pump excitation, the populations of all the states remain constant in the bare molecule. Since the nuclei are assumed frozen, charge dynamics shown in Figure 2a-f only arises from the electronic coherence. In an optical cavity, all polariton states mix. The original electronic coherence turns into a polaritonic coherence. Subsequently, the electronic populations become time-dependent and new electronic states may become active. As the coupling strength increases, the populations of states $|0\rangle$, $|1\rangle$ and $|2\rangle$ start to significantly oscillate in time (Figure 3b-d). Some inactive states such as $|7\rangle$ and $|8\rangle$ also show up in the charge dynamics bringing significant modifications to the corresponding charge migration processes. Separate contributions of each state are provided in Figure S3. The contribution of population dynamics to charge migration is a new feature induced by the optical cavity and does not exist in the bare molecule. The polaritonic charge dynamics arises from both the cavity modifications to electronic coherence and population dynamics.

Figure 4 depicts the TR-XRD signals of the bare and the cavity-embedded dendrimer with a g = 0.103 *V*/Å coupling strength. The signals are similar at short times (Figure 4a,b and g,h). Notable differences between the bare and cavity-embedded molecules emerge after 5.2 fs. This is consistent with the time-resolved difference charge densities shown in Figure 2. New charge migration features result in new strong signals (Figure 4j,k) that are absent in the bare molecule (Figure 4d,e). Cavity modification of the charge dynamics can thus be clearly imaged by TR-XRD signals.

To explore the generality of cavity manipulation of charge migration, we have applied the same approach to a larger dendrimer $C_{54}H_{30}$ with three branches (see Figure S4). A 3 to 8 fs time scale is selected for both the $C_{30}H_{18}$ (two-branched) and $C_{54}H_{30}$ (three-branched) dendrimers according to the ultrafast nature of the attosecond charge migration. The pure

https://doi.org/10.1021/jacs.4c06727
J. Am. Chem. Soc. 2024, 146, 26743−26750

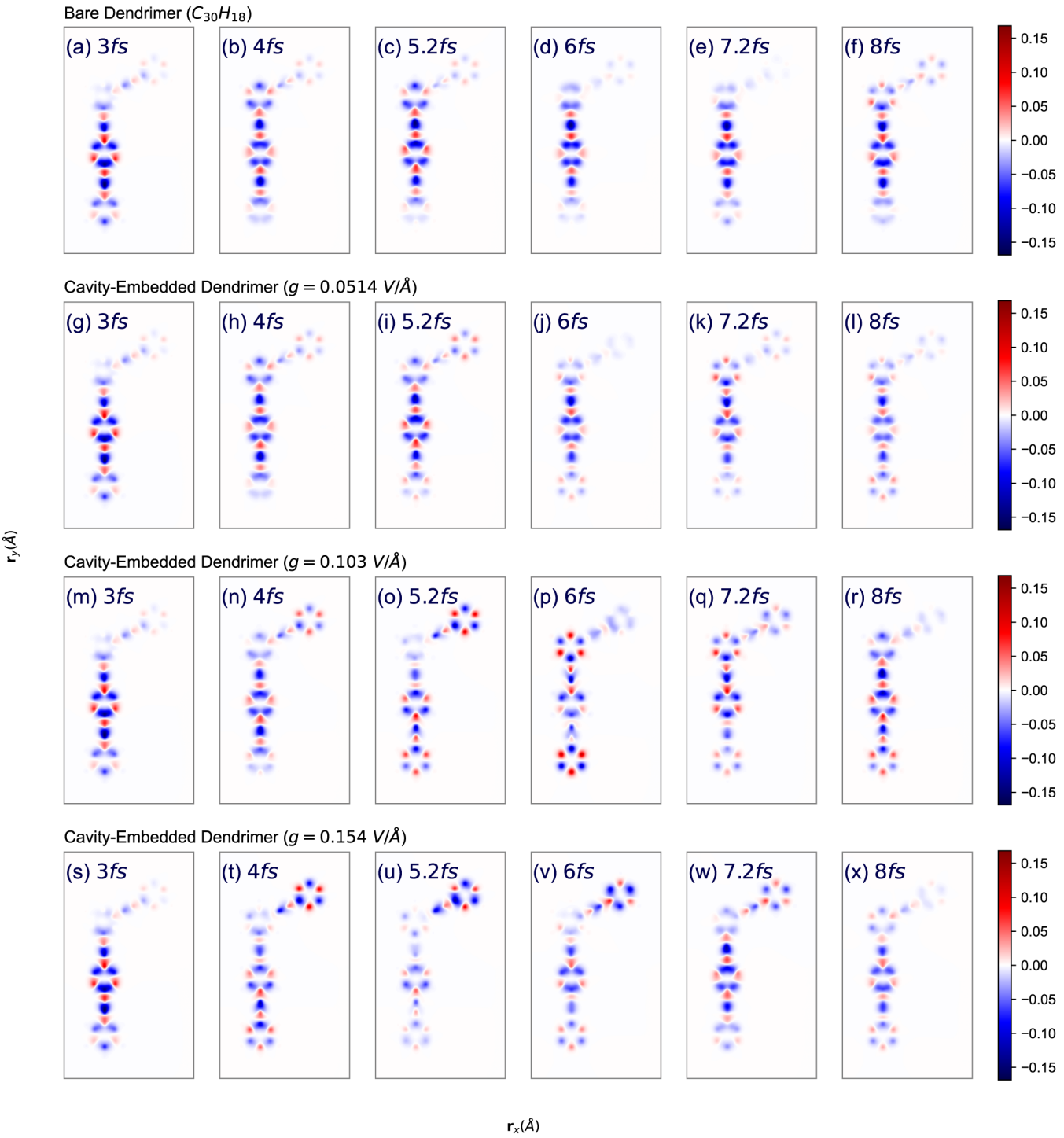

Figure 2. (a–f) Time-dependent charge density difference of excited bare dendrimer $C_{30}H_{18}$. Polaritonic time-dependent charge density differences of this dendrimer coupled with cavity with coupling strengths g = 0.0514 $V/Å$ (g–l), 0.103 $V/Å$ (m–r), and 0.154 $V/Å$ (s–x). The cavity frequency ω_c = 3.559 eV. All density differences are integrated in the z-axis direction.

electronic charge dynamics should disappear at longer time scales due to the participation of nuclear dynamics. Figure 5a-d shows the difference charge densities of the bare dendrimer at selected times t. Charge migration mainly occurs between two branches and there is no significant charge migration into the third one. Figure 5e-h shows the difference charge densities of $C_{54}H_{30}$ coupled to an optical cavity with coupling strength g = 0.0514 $V/Å$ and ω_c = 3.559 eV at selected times t. The polaritonic charge dynamics is significantly modulated compared to Figure 5a-d. Global charge migration mode involving all branches is now activated. Figure 6 compares the TR-XRD signals of the bare and the cavity-embedded $C_{54}H_{30}$ dendrimer. The differences between the charge dynamics can be clearly tracked in the momentum space.

Our results demonstrate that polaritons in optical cavities can activate the excited-state charge dynamics in dendritic structures across meta-substitutions. Many theoretical and experimental studies have shown that photoinduced dynamics

https://doi.org/10.1021/jacs.4c06727
J. Am. Chem. Soc. 2024, 146, 26743−26750

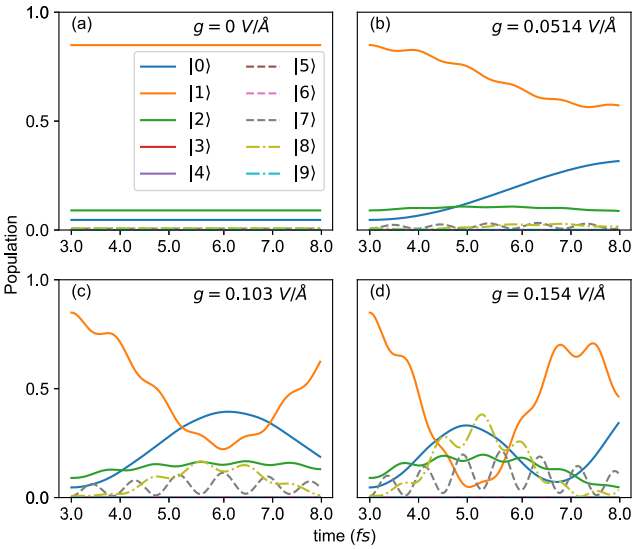

Figure 3. Population dynamics with various coupling strengths. The cavity frequency of (a–d) is 3.559 *eV*, and the coupling strengths are 0, 0.0514, 0.103, 0.154 *V*/Å, respectively.

of conjugated dendrimers are localized within segments connected by benzene rings substituted at the meta-position.[11,13,48] Ultrafast absorption also shows that meta-substitutions of disubstituted benzene exhibit the most hindered excited-state charge dynamics, compared to ortho- and para-substitutions.[49] As shown in Figure 2a–f and 5a–d, our dynamical simulations of charge evolution in two bare interstitial dendrimer molecules agree with these findings. However, in an optical cavity, the suppressed long-range electronic delocalization and charge migration can be activated. Recent study implies that ultrafast charge dynamics does not show effects extended over many molecules.[43] Thus, cavity modification of molecular charge migration cannot be enhanced by collective strong coupling. In this study, we show that the charge migration processes in conjugated dendrimers can be significantly modified with a relatively weak cavity coupling strength (2% of the cavity frequency), which is achievable by a single molecule strong coupling with no cooperativity. Polaritons in optical cavities thus have the potential to alter the charge dynamics in a broad range of conjugated species.

CONCLUSIONS

Our computational study explores the initial stages of coherent electronic dynamics in conjugated dendrimers subjected to polaritonic effects. We have shown that attosecond charge migration in molecules can be significantly manipulated by coupling to optical cavities. While meta-linkages suppress spatial electronic delocalization and charge migration mode in a bare molecule, our polaritonic simulations of charge dynamics in dendrimers demonstrate that this limitation is alleviated and charge migration can be significantly amplified. This important observation is substantiated by population analysis of the electronic states to explicitly show how the charge migration process is affected by light-matter coupling. Representative applications to two dendrimer molecules with two and three branch geometries emphasize generality of the phenomenon. Simulating time-resolved X-ray diffraction signals to monitor the modulated ultrafast charge dynamics in momentum space provide direct link to potential attosecond experiments. Our modeling suggests to potential novel use of optical cavities to control molecular photochemistry and photophysics by manipulating the initial coherent charge

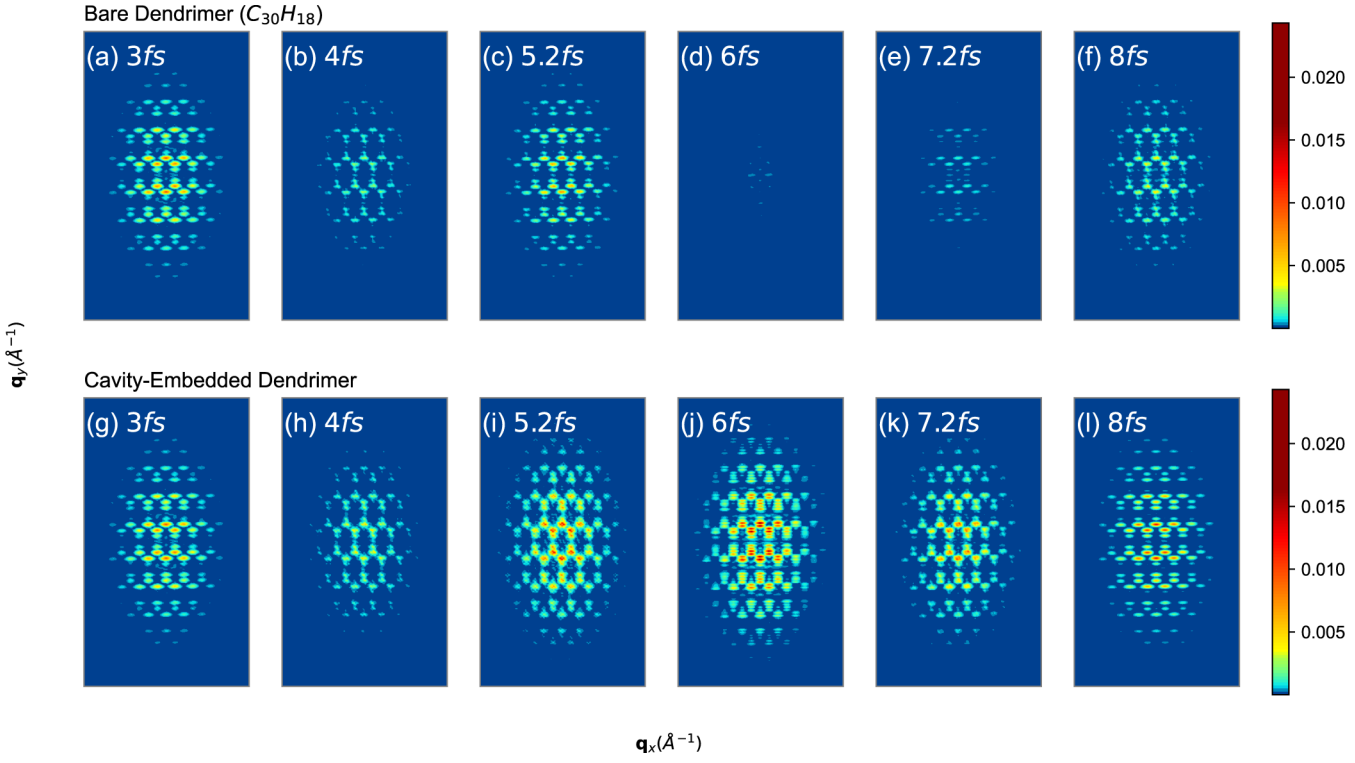

Figure 4. (a–f) Time-reolved XRD of bare excited dendrimer $C_{30}H_{18}$. (g–l) Time-resolved XRD of this dendrimer embedded in a cavity, with frequency ω_c = 3.559 *eV*, the coupling strength g = 0.103 *V*/Å. The plane of molecule $C_{30}H_{18}$ is vertical to the *z*-axis.

https://doi.org/10.1021/jacs.4c06727
J. Am. Chem. Soc. 2024, 146, 26743–26750

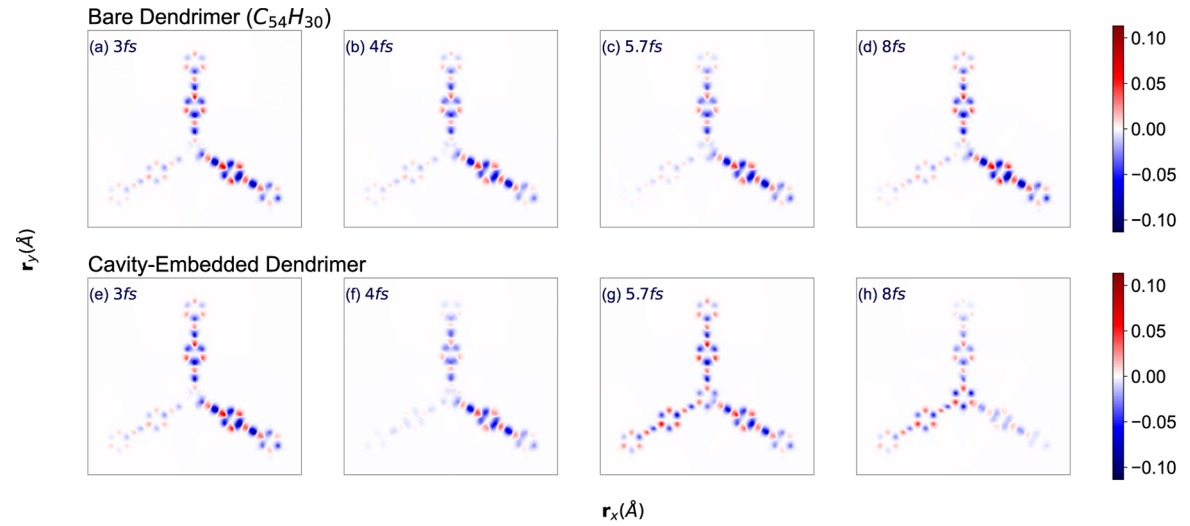

Figure 5. (a–d) Time-dependent charge density difference of excited dendrimer integrated in the z-axis direction $C_{54}H_{30}$. (e–h) Polariton-calculated time-dependent charge density difference of dendrimer ($C_{54}H_{30}$) coupled with cavity integrated in the z-axis direction, and the cavity frequency ω_c = 3.559eV, the coupling strength g = 0.0514 V/Å.

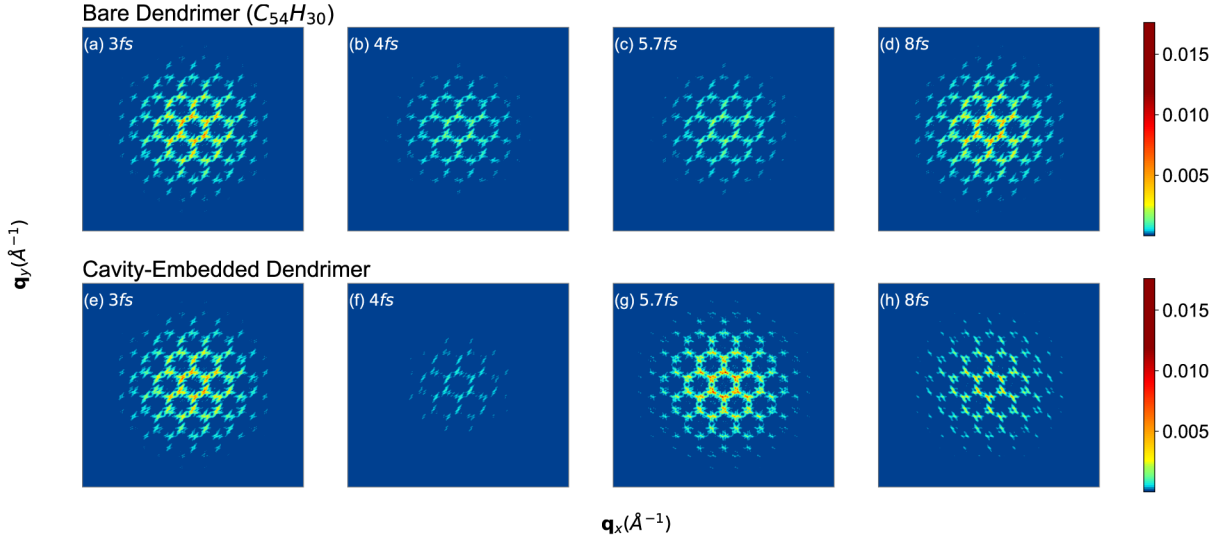

Figure 6. (a–d) Time-resolved XRD of bare excited dendrimer $C_{54}H_{30}$. (e–h) Time-resolved XRD of this dendrimer embedded in a cavity, with frequency ω_c = 3.559eV, the coupling strength g = 0.0514 V/Å. The plane of molecule $C_{54}H_{30}$ is vertical to the z-axis.

dynamics, which can be probed by contemporary attosecond spectroscopy techniques.

METHODS

Semiempirical Approach and Dendrimer Optimization. The electronic structure calculations in this work are based in the Collective Oscillator Approach[50] interfaced with the Austin Model 1 semiempirical approach[51] as implemented in the NEXMD code.[52,53] The analytical gradients[54] implemented in NEXMD were used to optimize the dendrimer structures in the ground state without the optical cavity interaction. The electronic structure level of theory implemented in NEXMD has shown to describe efficiently and accurately a wide range of conjugated molecules[55−57] and in particular dendrimers and dendrimer building blocks.[58−64]

ASSOCIATED CONTENT

Supporting Information

The Supporting Information is available free of charge at https://pubs.acs.org/doi/10.1021/jacs.4c06727.

Transition densities and population dynamics of $C_{30}H_{18}$ and $C_{54}H_{30}$, charge dynamics with different dissipation of $C_{30}H_{18}$, and charge dynamics of $C_{30}H_{18}$ embedded with single/two-mode cavities (PDF)

AUTHOR INFORMATION

Corresponding Authors

Yonghao Gu − *Department of Chemistry and Department of Physics and Astronomy, University of California, Irvine, Irvine, California 92697-2025, United States;* orcid.org/0000-0002-0868-6620; Email: yonghaog@uci.edu

Jun Jiang − *Key Laboratory of Precision and Intelligent Chemistry, University of Science and Technology of China, Hefei, Anhui 230026, China;* orcid.org/0000-0002-6116-5605; Email: jjiang1@ustc.edu.cn

Shaul Mukamel − *Department of Chemistry and Department of Physics and Astronomy, University of California, Irvine, Irvine, California 92697-2025, United States;* orcid.org/0000-0002-6015-3135; Email: smukamel@uci.edu

Authors

Baicheng Zhang − *Key Laboratory of Precision and Intelligent Chemistry, University of Science and Technology of China, Hefei, Anhui 230026, China; Department of Chemistry and Department of Physics and Astronomy, University of California, Irvine, Irvine, California 92697-2025, United States;* orcid.org/0000-0002-1899-028X

Victor Manuel Freixas − *Department of Chemistry and Department of Physics and Astronomy, University of California, Irvine, Irvine, California 92697-2025, United States;* orcid.org/0000-0003-1733-4827

Shichao Sun − *Department of Chemistry and Department of Physics and Astronomy, University of California, Irvine, Irvine, California 92697-2025, United States;* orcid.org/0000-0002-7680-3972

Sergei Tretiak − *Theoretical Division and Center for Integrated Nanotechnologies, Los Alamos National Laboratory, Los Alamos, New Mexico 87545, United States;* orcid.org/0000-0001-5547-3647

Complete contact information is available at: https://pubs.acs.org/10.1021/jacs.4c06727

Notes

The authors declare no competing financial interest.

■ ACKNOWLEDGMENTS

This work was primarily supported by the U.S. Department of Energy, Office of Science, Office of Basic Energy Sciences, grant. FG02-04ER15571. Y.G., V.M.F. and S.S. gratefully acknowledge the support of NSF grant CHE-2246379. The work at Los Alamos National Laboratory was performed in part at the Center for Integrated Nanotechnologies (CINT), a U.S. Department of Energy, Office of Science User Facility. J.J. and B.Z. gratefully acknowledge the support of the National Natural Science Foundation of China (22025304, 22033007).

■ REFERENCES

(1) Sun, H.-J.; Zhang, S.; Percec, V. From structure to function via complex supramolecular dendrimer systems. *Chem. Soc. Rev.* **2015**, *44*, 3900−3923.

(2) Nishiyama, N.; Morimoto, Y.; Jang, W.-D.; Kataoka, K. Design and development of dendrimer photosensitizer-incorporated polymeric micelles for enhanced photodynamic therapy. *Adv. Drug Delivery Rev.* **2009**, *61*, 327−338.

(3) Li, W.-J.; Wang, X.-Q.; Zhang, D.-Y.; Hu, Y.-X.; Xu, W.-T.; Xu, L.; Wang, W.; Yang, H.-B. Artificial Light-Harvesting Systems Based on AIEgen-branched Rotaxane Dendrimers for Efficient Photocatalysis. *Angew. Chem.* **2021**, *133*, 18909−18916.

(4) Ambekar, R. S.; Choudhary, M.; Kandasubramanian, B. Recent advances in dendrimer-based nanoplatform for cancer treatment: A review. *Eur. Polym. J.* **2020**, *126*, 109546.

(5) Tom, T.; Ros, E.; López-Vidrier, J.; Asensi, J. M.; Ortega, P.; Puigdollers, J.; Bertomeu, J.; Voz, C. Poly(amidoamine) Dendrimer as an Interfacial Dipole Modification in Crystalline Silicon Solar Cells. *J. Phys. Chem. Lett.* **2023**, *14*, 4322−4326.

(6) Balzani, V.; Ceroni, P.; Maestri, M.; Vicinelli, V. Light-harvesting dendrimers. *Curr. Opin. Chem. Biol.* **2003**, *7*, 657−665.

(7) Vonlanthen, M.; Cuétara-Guadarrama, F.; Sorroza-Martínez, K.; González-Méndez, I.; Estrada-Montaño, A. S.; Rivera, E. A review of porphyrin dendrimers as light-harvesting versatile platforms. *Dyes Pigm.* **2024**, *222*, 111873.

(8) Xun, Z.; Yu, T.; Zeng, Y.; Chen, J.; Zhang, X.; Yang, G.; Li, Y. Artificial photosynthesis dendrimers integrating light-harvesting, electron delivery and hydrogen production. *J. Mater. Chem. A* **2015**, *3*, 12965−12971.

(9) Pérez-Ferreiro, M.; Abelairas, A. M.; Criado, A.; Gómez, I. J.; Mosquera, J. Dendrimers: exploring their wide structural variety and applications. *Polymers* **2023**, *15*, 4369.

(10) Kuroda, D. G.; Singh, C.; Peng, Z.; Kleiman, V. D. Mapping excited-state dynamics by coherent control of a dendrimer's photoemission efficiency. *Science* **2009**, *326*, 263−267.

(11) Dani, R.; Makri, N. Excitation energy transfer in bias-free dendrimers: Eigenstate structure, thermodynamics, and quantum evolution. *J. Phys. Chem. C* **2022**, *126*, 10309−10319.

(12) Adronov, A.; Fréchet, J. M. Light-harvesting dendrimers. *Chem. Commun.* **2000**, 1701−1710.

(13) Tretiak, S.; Chernyak, V.; Mukamel, S. Localized Electronic Excitations in Phenylacetylene Dendrimers. *J. Phys. Chem. B* **1998**, *102*, 3310−3315.

(14) Aguilera, M. C.; Roitberg, A. E.; Kleiman, V. D.; Fernandez-Alberti, S.; Galindo, J. F. Unraveling direct and indirect energy transfer pathways in a light-harvesting dendrimer. *J. Phys. Chem. C* **2020**, *124*, 22383−22391.

(15) Nelson, T. R.; Ondarse-Alvarez, D.; Oldani, N.; Rodriguez-Hernandez, B.; Alfonso-Hernandez, L.; Galindo, J. F.; Kleiman, V. D.; Fernandez-Alberti, S.; Roitberg, A. E.; Tretiak, S. Coherent exciton-vibrational dynamics and energy transfer in conjugated organics. *Nat. Commun.* **2018**, *9* (1), 2316.

(16) Cederbaum, L.; Zobeley, J. Ultrafast charge migration by electron correlation. *Chem. Phys. Lett.* **1999**, *307*, 205−210.

(17) Leone, S. R.; McCurdy, C. W.; Burgdörfer, J.; Cederbaum, L. S.; Chang, Z.; Dudovich, N.; Feist, J.; Greene, C. H.; Ivanov, M.; Kienberger, R.; et al. What will it take to observe processes in'real time'? *Nat. Photonics* **2014**, *8*, 162−166.

(18) Goulielmakis, E.; Loh, Z.-H.; Wirth, A.; Santra, R.; Rohringer, N.; Yakovlev, V. S.; Zherebtsov, S.; Pfeifer, T.; Azzeer, A. M.; Kling, M. F.; et al. Real-time observation of valence electron motion. *Nature* **2010**, *466*, 739−743.

(19) Calegari, F.; Ayuso, D.; Trabattoni, A.; Belshaw, L.; De Camillis, S.; Anumula, S.; Frassetto, F.; Poletto, L.; Palacios, A.; Decleva, P.; Greenwood, J. B.; Martín, F.; Nisoli, M. Ultrafast electron dynamics in phenylalanine initiated by attosecond pulses. *Science* **2014**, *346* (6207), 336−339.

(20) Wörner, H. J.; Arrell, C. A.; Banerji, N.; Cannizzo, A.; Chergui, M.; Das, A. K.; Hamm, P.; Keller, U.; Kraus, P. M.; Liberatore, E. Charge migration and charge transfer in molecular systems. *Struct. Dyn.* **2017**, *4*, 061508.

(21) Guo, Y.; Zhou, Q.; Nan, J.; Shi, W.; Cui, F.; Zhu, Y. Perylenetetracarboxylic acid nanosheets with internal electric fields and anisotropic charge migration for photocatalytic hydrogen evolution. *Nat. Commun.* **2022**, *13* (1), 2067.

(22) Remacle, F.; Levine, R.; Ratner, M. Charge directed reactivity: a simple electronic model, exhibiting site selectivity, for the dissociation of ions. *Chem. Phys. Lett.* **1998**, *285*, 25−33.

(23) Weinkauf, R.; Schlag, E.; Martinez, T.; Levine, R. Nonstationary electronic states and site-selective reactivity. *J. Phys. Chem. A* **1997**, *101*, 7702−7710.

(24) Ebbesen, T. W. Hybrid light−matter states in a molecular and material science perspective. *Acc. Chem. Res.* **2016**, *49*, 2403−2412.

(25) Herrera, F.; Owrutsky, J. Molecular polaritons for controlling chemistry with quantum optics. *J. Chem. Phys.* **2020**, *152*, 100902.

(26) Sidler, D.; Schäfer, C.; Ruggenthaler, M.; Rubio, A. Polaritonic chemistry: Collective strong coupling implies strong local modification of chemical properties. *J. Phys. Chem. Lett.* **2021**, *12*, 508−516.

(27) Xiong, W. Molecular Vibrational Polariton Dynamics: What Can Polaritons Do? *Acc. Chem. Res.* **2023**, *56*, 776−786.

(28) Takahashi, S.; Watanabe, K. Decoupling from a thermal bath via molecular polariton formation. *J. Phys. Chem. Lett.* **2020**, *11*, 1349−1356.

(29) Coles, D. M.; Somaschi, N.; Michetti, P.; Clark, C.; Lagoudakis, P. G.; Savvidis, P. G.; Lidzey, D. G. Polariton-mediated energy transfer between organic dyes in a strongly coupled optical microcavity. *Nat. Mater.* **2014**, *13*, 712−719.

(30) Mewes, L.; Wang, M.; Ingle, R. A.; Börjesson, K.; Chergui, M. Energy relaxation pathways between light-matter states revealed by coherent two-dimensional spectroscopy. *Commun. Phys.* **2020**, *3* (1), 157.
(31) Gu, B.; Gu, Y.; Chernyak, V. Y.; Mukamel, S. Cavity Control of Molecular Spectroscopy and Photophysics. *Acc. Chem. Res.* **2023**, *56*, 2753−2762.
(32) Thomas, A.; Lethuillier-Karl, L.; Nagarajan, K.; Vergauwe, R. M.; George, J.; Chervy, T.; Shalabney, A.; Devaux, E.; Genet, C.; Moran, J.; et al. Tilting a ground-state reactivity landscape by vibrational strong coupling. *Science* **2019**, *363*, 615−619.
(33) Hutchison, J. A.; Schwartz, T.; Genet, C.; Devaux, E.; Ebbesen, T. W. Modifying chemical landscapes by coupling to vacuum fields. *Angew. Chem., Int. Ed.* **2012**, *51*, 1592−1596.
(34) Xiang, B.; Ribeiro, R. F.; Dunkelberger, A. D.; Wang, J.; Li, Y.; Simpkins, B. S.; Owrutsky, J. C.; Yuen-Zhou, J.; Xiong, W. Two-dimensional infrared spectroscopy of vibrational polaritons. *Proc. Natl. Acad. Sci. U. S. A.* **2018**, *115*, 4845−4850.
(35) Polak, D.; Jayaprakash, R.; Lyons, T. P.; Martínez-Martínez, L. Á.; Leventis, A.; Fallon, K. J.; Coulthard, H.; Bossanyi, D. G.; Georgiou, K.; Petty, A. J., II Manipulating molecules with strong coupling: harvesting triplet excitons in organic exciton microcavities. *Chem. Sci.* **2020**, *11* (2), 343−354.
(36) Eizner, E.; Martínez-Martínez, L. A.; Yuen-Zhou, J.; Kéna-Cohen, S. Inverting singlet and triplet excited states using strong light-matter coupling. *Sci. Adv.* **2019**, *5* (12), No. eaax4482.
(37) Xiang, B.; Ribeiro, R. F.; Du, M.; Chen, L.; Yang, Z.; Wang, J.; Yuen-Zhou, J.; Xiong, W. Intermolecular vibrational energy transfer enabled by microcavity strong light−matter coupling. *Science* **2020**, *368*, 665−667.
(38) Chen, T.-T.; Du, M.; Yang, Z.; Yuen-Zhou, J.; Xiong, W. Cavity-enabled enhancement of ultrafast intramolecular vibrational redistribution over pseudorotation. *Science* **2022**, *378*, 790−794.
(39) Gu, B.; Nenov, A.; Segatta, F.; Garavelli, M.; Mukamel, S. Manipulating core excitations in molecules by x-ray cavities. *Phys. Rev. Lett.* **2021**, *126*, 053201.
(40) Cho, D.; Gu, B.; Mukamel, S. Optical Cavity Manipulation and Nonlinear UV Molecular Spectroscopy of Conical Intersections in Pyrazine. *J. Am. Chem. Soc.* **2022**, *144*, 7758−7767.
(41) Gu, B.; Cavaletto, S. M.; Nascimento, D. R.; Khalil, M.; Govind, N.; Mukamel, S. Manipulating valence and core electronic excitations of a transition-metal complex using UV/Vis and X-ray cavities. *Chem. Sci.* **2021**, *12*, 8088−8095.
(42) Sun, S.; Gu, B.; Mukamel, S. Polariton ring currents and circular dichroism of Mg-porphyrin in a chiral cavity. *Chem. Sci.* **2022**, *13*, 1037−1048.
(43) Gu, Y.; Gu, B.; Sun, S.; Yong, H.; Chernyak, V. Y.; Mukamel, S. Manipulating Attosecond Charge Migration in Molecules by Optical Cavities. *J. Am. Chem. Soc.* **2023**, *145*, 14856−14864.
(44) Cho, D.; Rouxel, J. R.; Kowalewski, M.; Lee, J. Y.; Mukamel, S. Attosecond X-ray Diffraction Triggered by Core or Valence Ionization of a Dipeptide. *J. Chem. Theory Comput.* **2018**, *14*, 329−338.
(45) Yong, H.; Sun, S.; Gu, B.; Mukamel, S. Attosecond Charge Migration in Molecules Imaged by Combined X-ray and Electron Diffraction. *J. Am. Chem. Soc.* **2022**, *144*, 20710−20716.
(46) Chikkaraddy, R.; de Nijs, B.; Benz, F.; Barrow, S. J.; Scherman, O. A.; Rosta, E.; Demetriadou, A.; Fox, P.; Hess, O.; Baumberg, J. J. Single-molecule strong coupling at room temperature in plasmonic nanocavities. *Nature* **2016**, *535*, 127−130.
(47) Hugall, J. T.; Singh, A.; van Hulst, N. F. Plasmonic cavity coupling. *ACS Photonics* **2018**, *5*, 43−53.
(48) Gaab, K. M.; Thompson, A. L.; Xu, J.; Martínez, T. J.; Bardeen, C. J. Meta-Conjugation and Excited-State Coupling in Phenylacetylene Dendrimers. *J. Am. Chem. Soc.* **2003**, *125*, 9288−9289.
(49) Nie, X.; Su, H.; Wang, T.; Miao, H.; Chen, B.; Zhang, G. Aromatic Electrophilic Directing for Fluorescence and Room-Temperature Phosphorescence Modulation. *J. Phys. Chem. Lett.* **2021**, *12*, 3099−3105.
(50) Tretiak, S.; Mukamel, S. Density Matrix Analysis and Simulation of Electronic Excitations in Conjugated and Aggregated Molecules. *Chem. Rev.* **2002**, *102*, 3171−3212.
(51) Dewar, M. J. S.; Zoebisch, E. G.; Healy, E. F.; Stewart, J. J. P. Development and use of quantum mechanical molecular models. 76. AM1: a new general purpose quantum mechanical molecular model. *J. Am. Chem. Soc.* **1985**, *107*, 3902−3909.
(52) Malone, W.; Nebgen, B.; White, A.; Zhang, Y.; Song, H.; Bjorgaard, J. A.; Sifain, A. E.; Rodriguez-Hernandez, B.; Freixas, V. M.; Fernandez-Alberti, S.; Roitberg, A. E.; Nelson, T. R.; Tretiak, S. NEXMD Software Package for Nonadiabatic Excited State Molecular Dynamics Simulations. *J. Chem. Theory Comput.* **2020**, *16*, 5771−5783.
(53) Freixas, V. M.; et al. NEXMD v2.0 Software Package for Nonadiabatic Excited State Molecular Dynamics Simulations. *J. Chem. Theory Comput.* **2023**, *19*, 5356−5368.
(54) Furche, F.; Ahlrichs, R. Adiabatic time-dependent density functional methods for excited state properties. *J. Chem. Phys.* **2002**, *117*, 7433−7447.
(55) Nelson, T.; Fernandez-Alberti, S.; Roitberg, A. E.; Tretiak, S. Nonadiabatic Excited-State Molecular Dynamics: Modeling Photophysics in Organic Conjugated Materials. *Acc. Chem. Res.* **2014**, *47*, 1155−1164.
(56) Nelson, T.; Fernandez-Alberti, S.; Chernyak, V.; Roitberg, A. E.; Tretiak, S. Nonadiabatic Excited-State Molecular Dynamics Modeling of Photoinduced Dynamics in Conjugated Molecules. *J. Phys. Chem. B* **2011**, *115*, 5402−5414.
(57) Nelson, T. R.; White, A. J.; Bjorgaard, J. A.; Sifain, A. E.; Zhang, Y.; Nebgen, B.; Fernandez-Alberti, S.; Mozyrsky, D.; Roitberg, A. E.; Tretiak, S. Non-adiabatic Excited-State Molecular Dynamics: Theory and Applications for Modeling Photophysics in Extended Molecular Materials. *Chem. Rev.* **2020**, *120*, 2215−2287.
(58) Fernandez-Alberti, S.; Kleiman, V. D.; Tretiak, S.; Roitberg, A. E. Nonadiabatic Molecular Dynamics Simulations of the Energy Transfer between Building Blocks in a Phenylene Ethynylene Dendrimer. *J. Phys. Chem. A* **2009**, *113*, 7535−7542.
(59) Fernandez-Alberti, S.; Roitberg, A. E.; Kleiman, V. D.; Nelson, T.; Tretiak, S. Shishiodoshi unidirectional energy transfer mechanism in phenylene ethynylene dendrimers. *J. Chem. Phys.* **2012**, *137* (22), 22A526.
(60) Freixas, V. M.; Ondarse-Alvarez, D.; Tretiak, S.; Makhov, D. V.; Shalashilin, D. V.; Fernandez-Alberti, S. Photoinduced non-adiabatic energy transfer pathways in dendrimer building blocks. *J. Chem. Phys.* **2019**, *150* (12), 124301.
(61) Freixas, V. M.; Keefer, D.; Tretiak, S.; Fernandez-Alberti, S.; Mukamel, S. Ultrafast coherent photoexcited dynamics in a trimeric dendrimer probed by X-ray stimulated-Raman signals. *Chem. Sci.* **2022**, *13*, 6373−6384.
(62) Bonilla, V.; Freixas, V. M.; Fernandez-Alberti, S.; Fabian Galindo, J. F. Impact of the core on the inter-branch exciton exchange in dendrimers. *Phys. Chem. Chem. Phys.* **2023**, *25* (17), 12097−12106.
(63) Soler, M. A.; Roitberg, A. E.; Nelson, T.; Tretiak, S.; Fernandez-Alberti, S. Analysis of State-Specific Vibrations Coupled to the Unidirectional Energy Transfer in Conjugated Dendrimers. *J. Phys. Chem. A* **2012**, *116*, 9802−9810.
(64) Freixas, V. M.; White, A. J.; Nelson, T.; Song, H.; Makhov, D. V.; Shalashilin, D.; Fernandez-Alberti, S.; Tretiak, S. Nonadiabatic Excited-State Molecular Dynamics Methodologies: Comparison and Convergence. *J. Phys. Chem. Lett.* **2021**, *12*, 2970−2982.

https://doi.org/10.1021/jacs.4c06727
J. Am. Chem. Soc. 2024, 146, 26743−26750

Supporting Information of Cavity Manipulation of Attosecond Charge Migration in Conjugated Dendrimers

Baicheng Zhang,[†,‡] Yonghao Gu,[*,‡] Victor Manuel Freixas,[‡] Shichao Sun,[‡] Sergei Tretiak,[¶] Jun Jiang,[*,†] and Shaul Mukamel[*,‡]

†*Key Laboratory of Precision and Intelligent Chemistry, University of Science and Technology of China, Hefei, Anhui 230026, China*

‡*Department of Chemistry and Department of Physics and Astronomy, University of California, Irvine, Irvine, California 92697-2025, United States*

¶*Theoretical Division and Center for Integrated Nanotechnologies, Los Alamos National Laboratory, Los Alamos, New Mexico 87545, United States*

E-mail: yonghaog@uci.edu; jjiang1@ustc.edu.cn; smukamel@uci.edu

Figure S1 provide the transition densities $\langle 0|\,\hat{\sigma}\,|i\rangle$ between the ground state $|0\rangle$ and various excited states $|i\rangle$ of the bare molecule, states reflecting the density differences of those states from ground state. The energies of the excited states are $e_1 = 3.23$ eV, $e_2 = 3.56$ eV, $e_3 = 3.67$ eV, $e_4 = 3.72$ eV, $e_5 = 3.84$ eV, $e_6 = 3.84$ eV, $e_7 = 3085$ eV, $e_8 = 4.08$ eV, and $e_9 = 4.14$ eV, respectively.

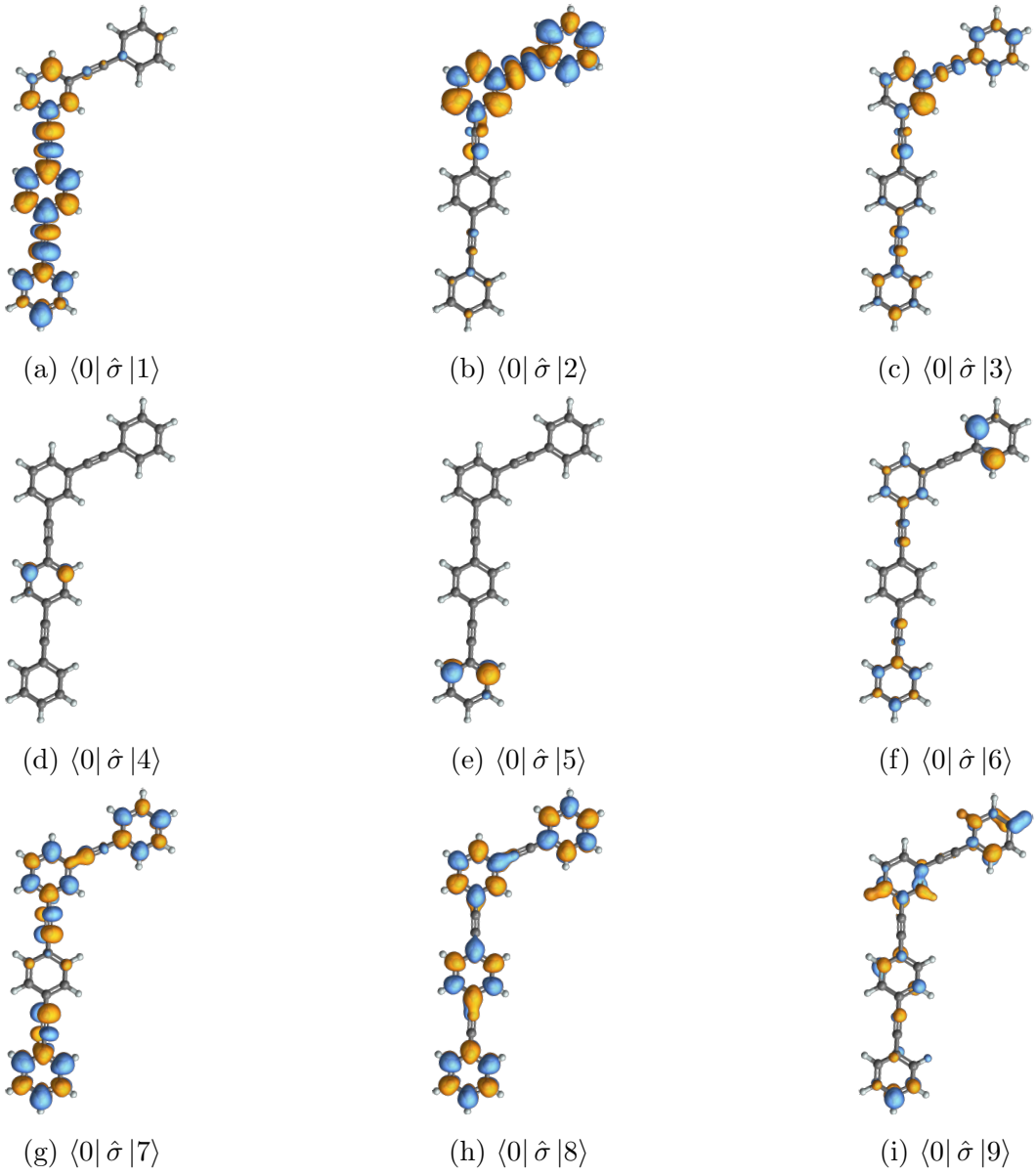

(a) $\langle 0|\,\hat{\sigma}\,|1\rangle$ (b) $\langle 0|\,\hat{\sigma}\,|2\rangle$ (c) $\langle 0|\,\hat{\sigma}\,|3\rangle$

(d) $\langle 0|\,\hat{\sigma}\,|4\rangle$ (e) $\langle 0|\,\hat{\sigma}\,|5\rangle$ (f) $\langle 0|\,\hat{\sigma}\,|6\rangle$

(g) $\langle 0|\,\hat{\sigma}\,|7\rangle$ (h) $\langle 0|\,\hat{\sigma}\,|8\rangle$ (i) $\langle 0|\,\hat{\sigma}\,|9\rangle$

Figure S1: Transition densities between the ground state $|0\rangle$ and various excited states of $C_{30}H_{18}$. States $|1\rangle$ through $|9\rangle$ correspond to the lowest nine excited states, respectively. $\hat{\sigma}$ is the density operator.

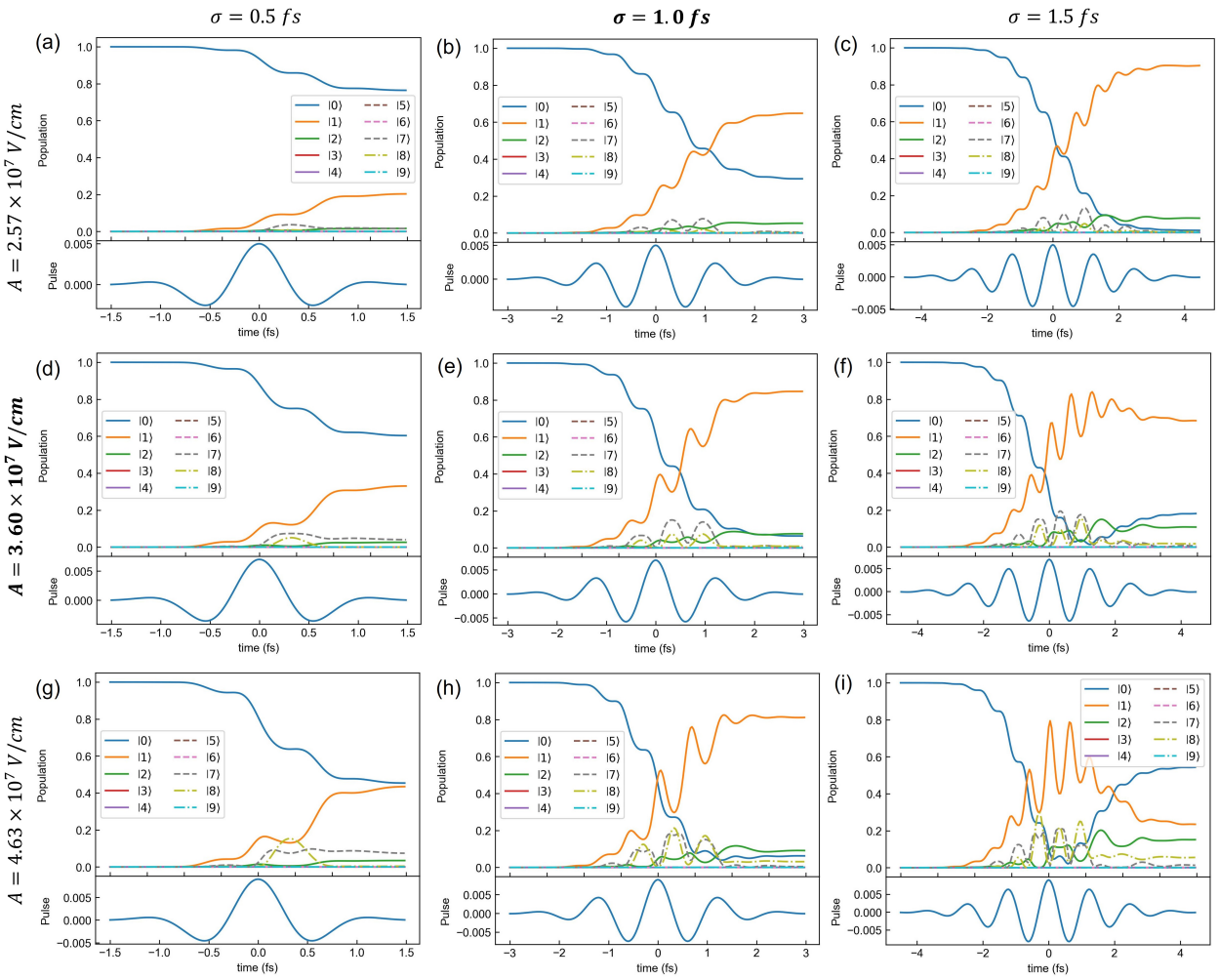

Figure S2: (a-c) Population dynamics excited by pump pulse of energy $\omega_0 = 3.30$ eV, duration $\sigma = 0.5$ fs, 1.0 fs, 1.5 fs, and amplitude $A = 2.60 \times 10^7$ V/cm. Same for the amplitude 3.60×10^7 V/cm. (g-i) Same for the amplitude 4.60×10^7 V/cm.

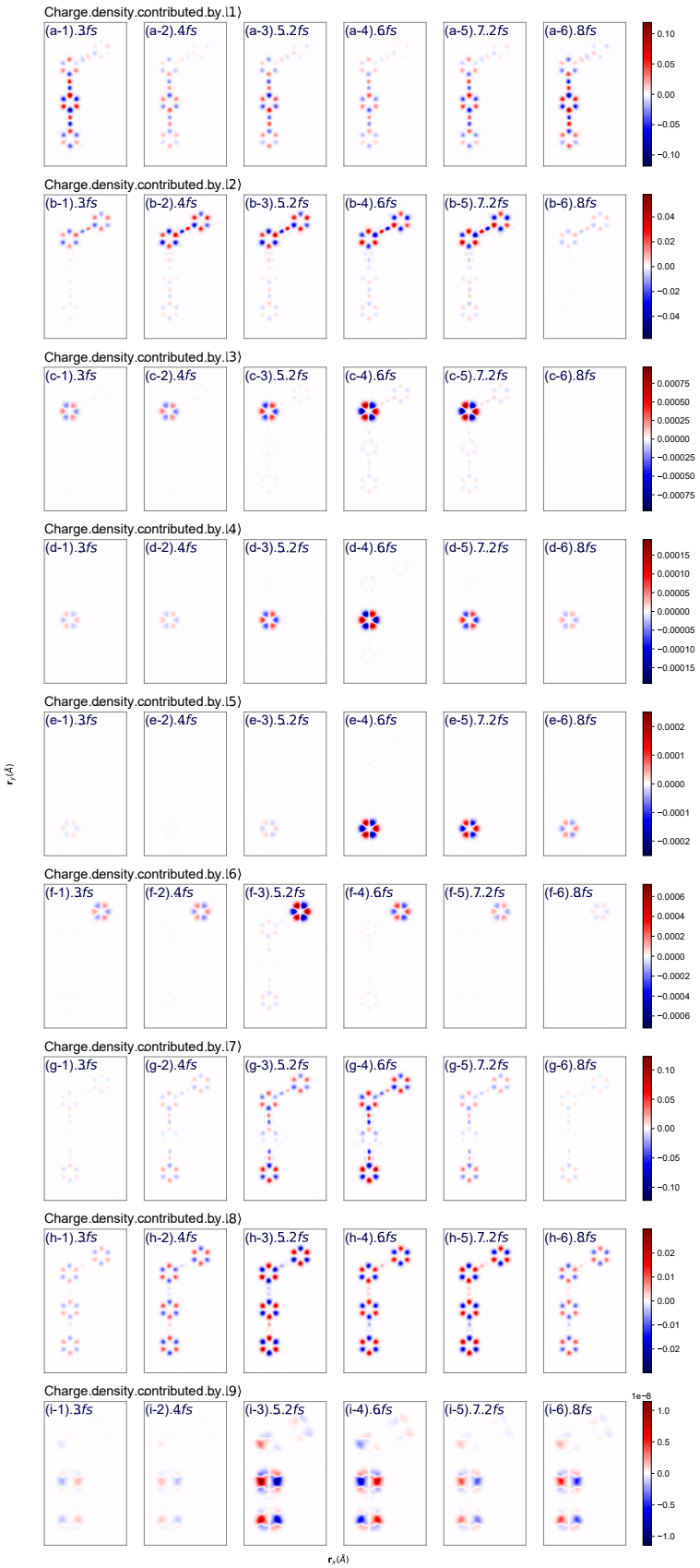

Figure S3: Separate contributions of population dynamics of all relevant excited states to the charge dynamics in Figure 3(m-r).

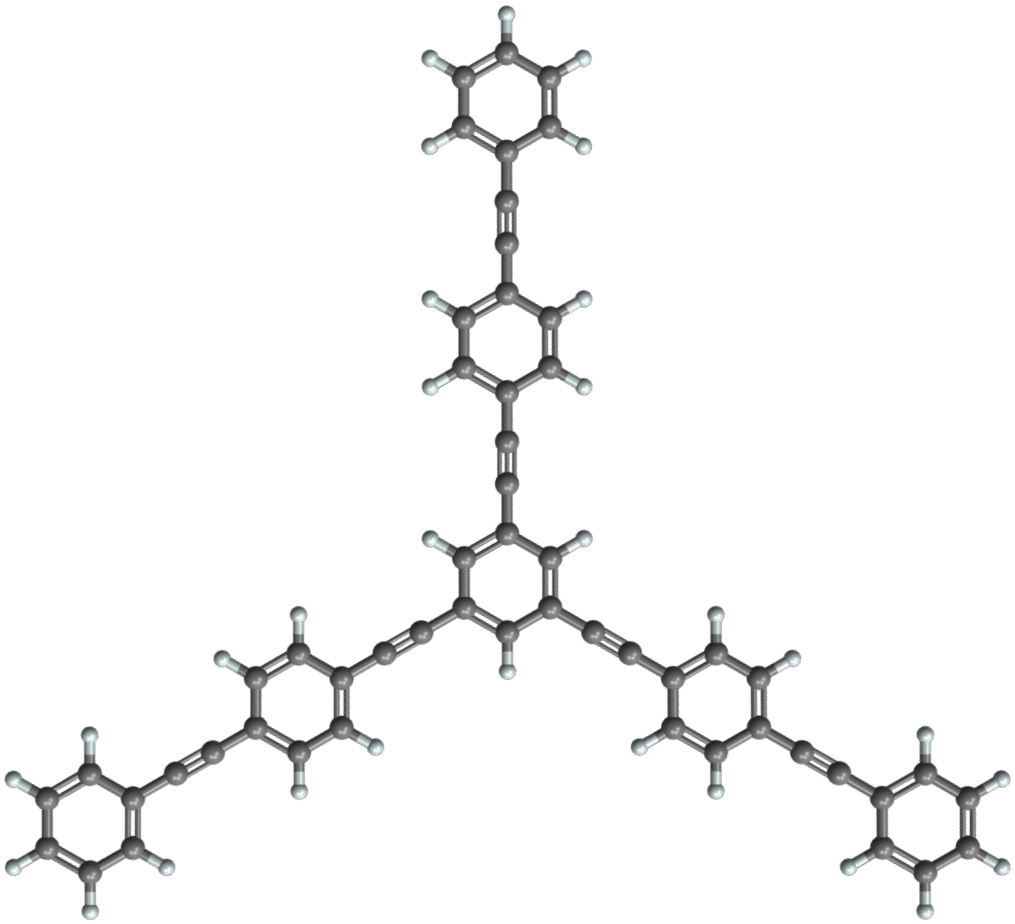

Figure S4: Geometric structure of $C_{54}H_{30}$

Figure S5 provides the transition densities $\langle 0|\,\hat{\sigma}\,|i\rangle$ between the ground state $|0\rangle$ and various excited states $|i\rangle$ of the bare molecule.

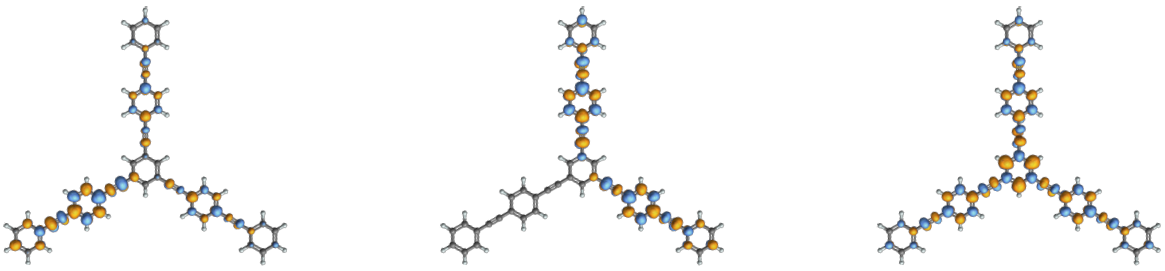

(a) $\langle 0|\,\hat{\sigma}\,|1\rangle$ (b) $\langle 0|\,\hat{\sigma}\,|2\rangle$ (c) $\langle 0|\,\hat{\sigma}\,|3\rangle$

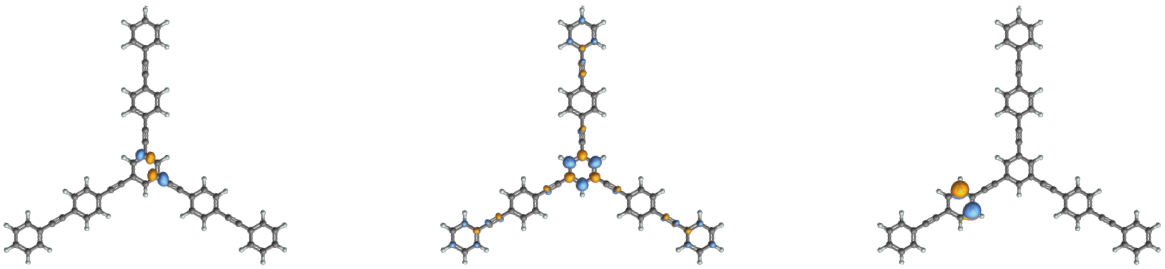

(d) $\langle 0|\,\hat{\sigma}\,|4\rangle$ (e) $\langle 0|\,\hat{\sigma}\,|5\rangle$ (f) $\langle 0|\,\hat{\sigma}\,|6\rangle$

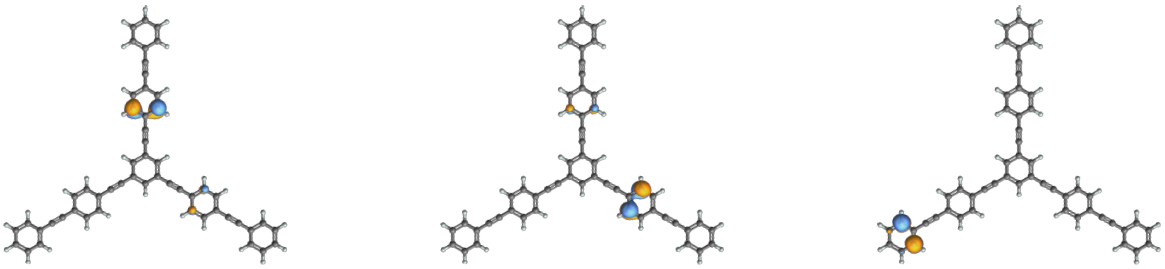

(g) $\langle 0|\,\hat{\sigma}\,|7\rangle$ (h) $\langle 0|\,\hat{\sigma}\,|8\rangle$ (i) $\langle 0|\,\hat{\sigma}\,|9\rangle$

Figure S5: Transition densities between the ground state and various excited states of $C_{54}H_{30}$. $|0\rangle$ represents the ground state. States $|1\rangle$ through $|9\rangle$ correspond to lowest nine excited states, respectively. $\hat{\sigma}$ is the density operator.

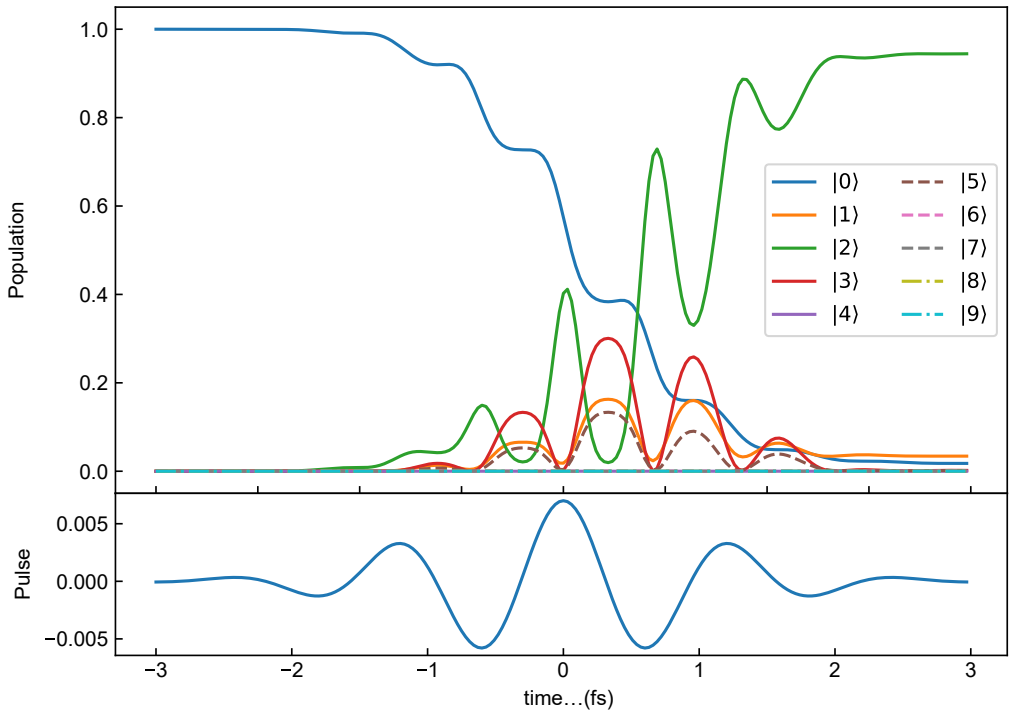

Figure S6: Population dynamics of $C_{54}H_{30}$ excited by a pump pulse with frequency $\omega_0 = 3.56\ eV$ and duration $\sigma = 1.5\ fs$.

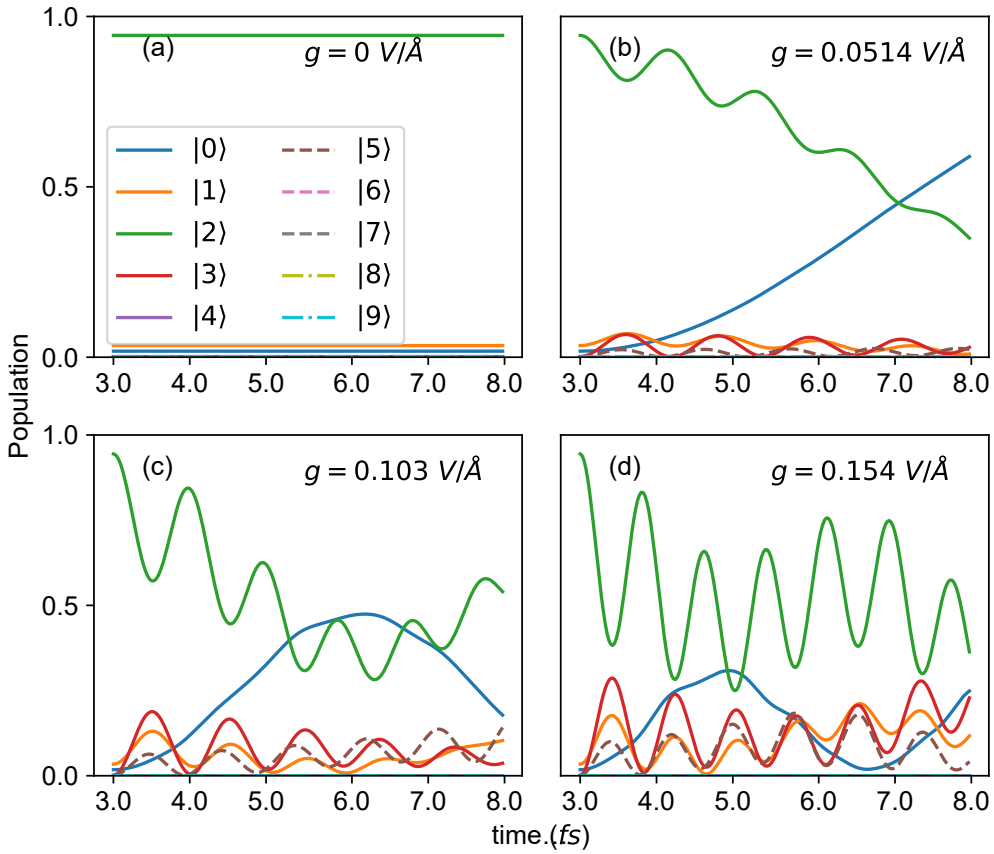

Figure S7: Population dynamics with coupling strength of $C_{54}H_{30}$. The cavity frequency of (a-d) is 3.559 eV, and the coupling strengths are 0, 0.0514, 0.103, 0.154 $V/\AA$, respectively.

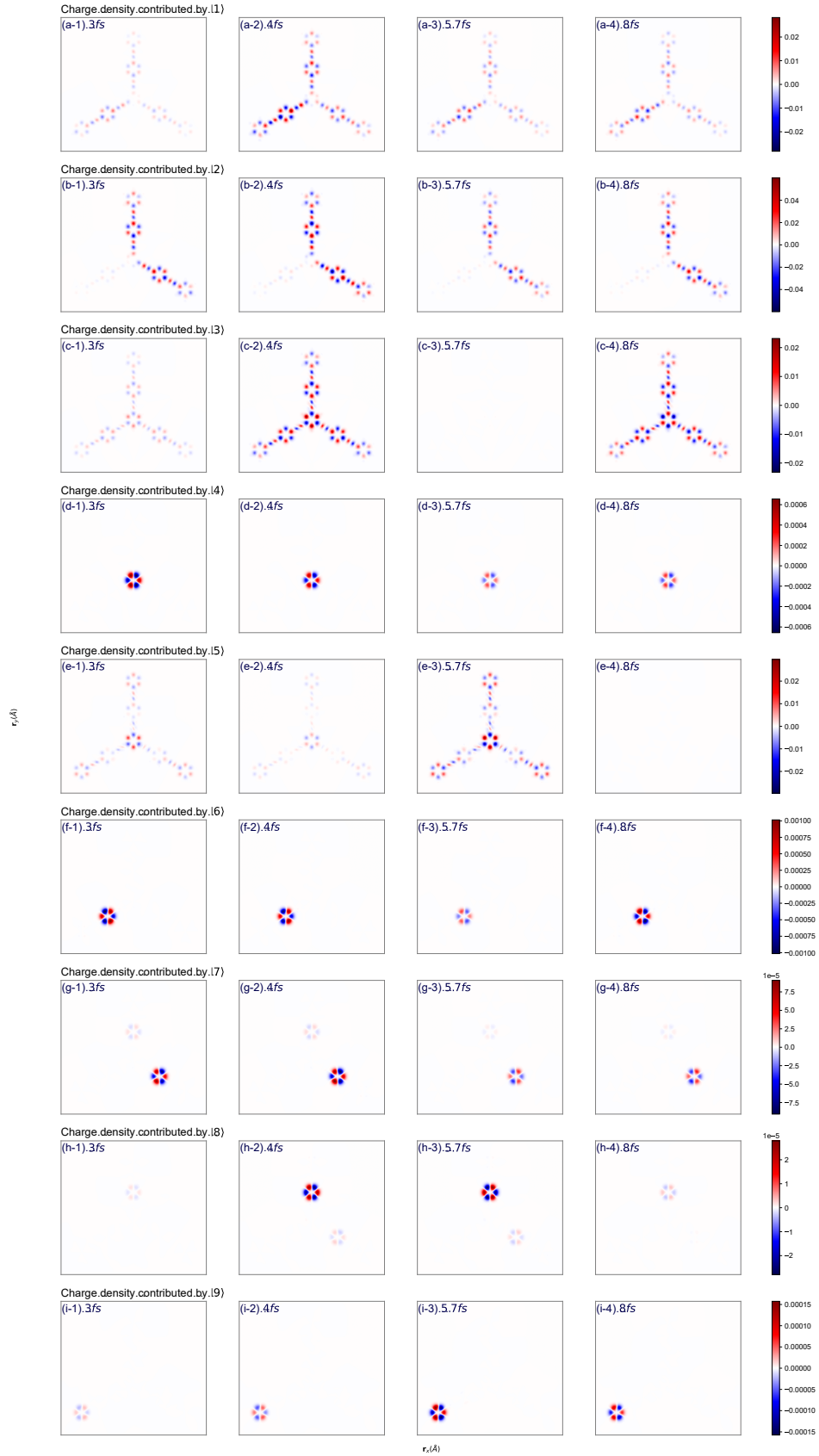

Figure S8: Separate contributions of population dynamics of all relevant excited states to the charge dynamics in Figure 5(e-h).

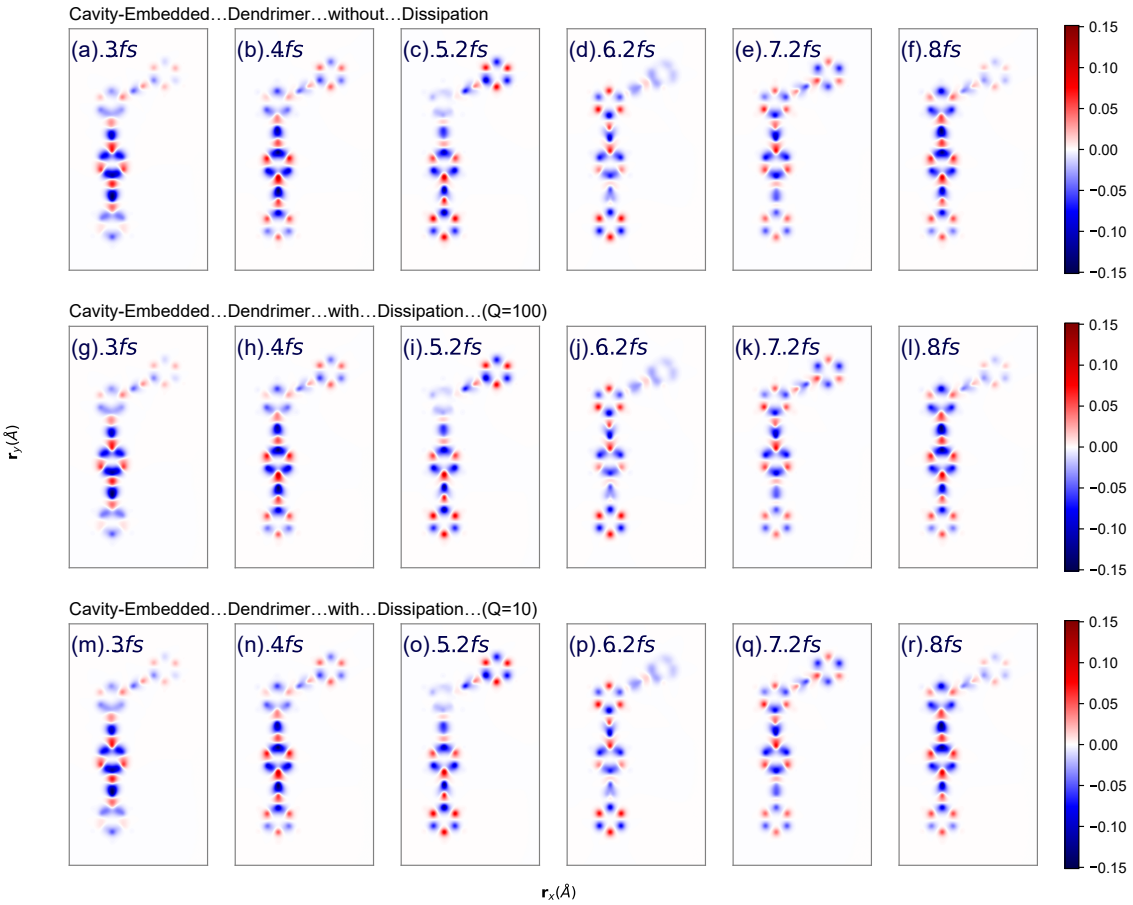

Figure S9: (a-f) Polaritonic time-dependent charge density difference of $C_{30}H_{18}$ coupled with cavity integrated in the z-axis direction, and the cavity frequency $\omega_c = 3.559\ eV$, the coupling strength $g = 0.103\ V/\AA$, the quality factor $Q = 1000$. (g-l) Same for the quality factor $Q = 100$. (m-r) Same for the quality factor $Q = 10$.

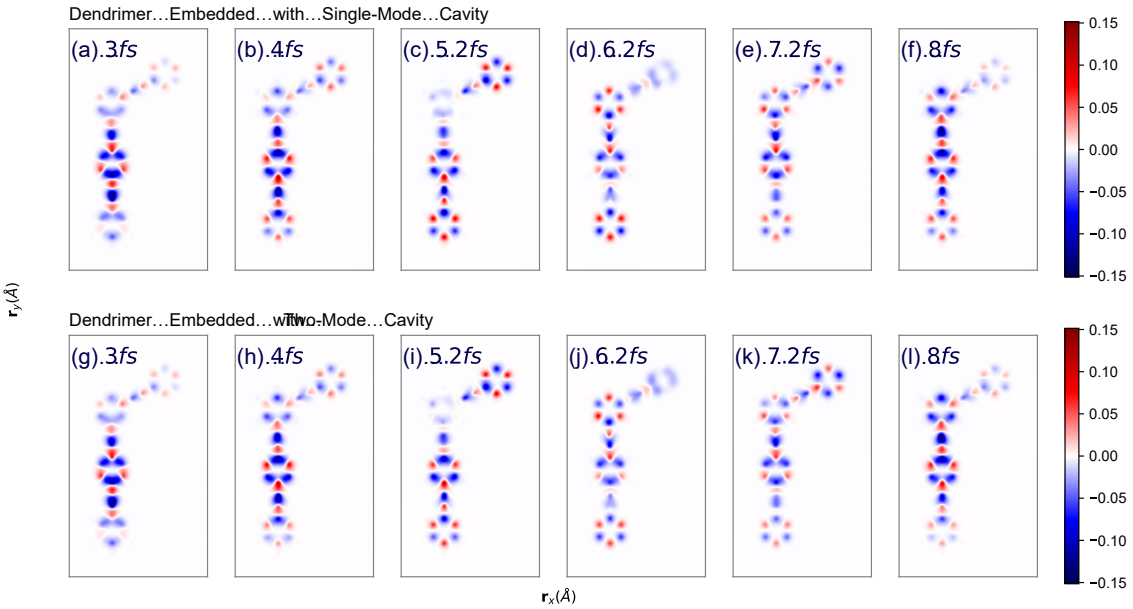

Figure S10: (a-f) Polaritonic time-dependent charge density difference of this dendrimer coupled with single-photon mode of cavity integrated in the z-axis direction, and the cavity frequency $\omega_c = 3.559\ eV$, the coupling strength $g = 0.103\ V/\mathring{A}$. (g-l) Same for the two-photon mode of cavity included.